International Journal of Micro Air Vehicles

Original Research

International Journal of Micro Air Vehicles
Volume 12: 1–14

DOI: 10.1177/1756829320923563
journals.sagepub.com/home/mav
SAGE

Optimal attitude tracking control for an unmanned aerial quadrotor under lumped disturbances

Li Ding[1,2] and Yangmin Li[2]

Abstract

The robust control problem in attitude tracking of an unmanned aerial vehicle quadrotor is a challenging task due to strong parametric uncertainties, large nonlinearities and high couplings in flight dynamics. In this paper, a continuous nonsingular fast terminal sliding mode controller based on linear extended state observer is proposed for attitude tracking control of a quadrotor under lumped disturbances. The proposed control method requires no prior knowledge of the attitude dynamics. It can ensure rapid convergence rate and high tracking precision due to terminal sliding mode surface and fast reaching law. The controller uses the linear extended state observer to reject the influence of both parametric uncertainties and external disturbances. Meanwhile, the nonsingular fast terminal sliding mode control strategy is designed to ensure the state variables to slide to desired points in finite time. To enhance the control performance, a self-adaptive fruit fly optimization algorithm is applied to parameters tuning of the proposed controller. The effectiveness of the proposed control approach is illustrated through numerical simulations and experimental verification.

Keywords

Quadrotor, attitude tracking control, terminal sliding mode, linear extended state observer, fruit fly optimization algorithm

Date received: 5 March 2019; accepted: 3 April 2020

Introduction

As a typical aerial robot, quadrotor has major advantages when used for aerial photography, environmental monitoring and surveillance in dangerous and complex environments.[1–3] Indeed, quadrotors have gained much attention in the academic community since their complex nonlinear dynamic characteristics offer a challenge for flight control designers. Much effort has been made to search advanced robust control approaches, such as model predictive control,[4] adaptive control,[5] backstepping control,[6] sliding mode control (SMC)[7] and neural network methods.[8] In the formulation of aircraft control problem, there will always be a discrepancy between the actual system and its mathematical model used for the controller design. These discrepancies or mismatches arise from lumped disturbances, i.e. unknown environment effects, parameter drift and unmodelled dynamics. The lumped disturbances will bring extra difficulty for the above controller design, which may greatly limit the application of controllers in practice.

Developing disturbance estimation techniques would be a good choice to alleviate the restriction faced by the traditional robust controller design. The main idea of disturbance estimation techniques is to use an effective disturbance observer to estimate the lumped disturbances of the system and compensate them in control law.[9] A disturbance observer can improve the tracking performance for the controllers and show satisfactory disturbance attenuation and robustness against uncertainties. Hence, many control methods have combined disturbance observer to

[1]College of Mechanical Engineering, Jiangsu University of Technology, Changzhou, China
[2]Department of Industrial and Systems Engineering, The Hong Kong Polytechnic University, Hong Kong, China

Corresponding author:
Li Ding, College of Mechanical Engineering, Jiangsu University of Technology, Changzhou 213000, China.
Email: nuaadli@163.com

process the undesirable effects caused by lumped disturbances, especially in quadrotor control issue. Dong et al.[10] combined backstepping control and nonlinear disturbance observer for high-performance trajectory tracking control of a quadrotor. Similarly, Chen et al.[11] constructed a nonlinear disturbance observer separately from backstepping controller to reject external disturbances. The effectiveness and robustness of these controllers had been verified in simulation. But it is also noticed that the nonlinear disturbance observer always has an unsatisfactory practical application due to the complex structure. Furthermore, Ma et al.[12] used a high-gain disturbance observer to enhance the robustness of a fault tolerant controller for quadrotor model uncertainties. However, this method requires rather high control energy to achieve fast-tracking and disturbance rejection performance. To overcome the above disadvantages, this paper uses the linear extended state observer (LESO) as a disturbance observer to estimate the lumped disturbances. With a simple structure, LESO relies only on an observer bandwidth to decide the ability of disturbance estimation.[13]

SMC uses a discontinuous control signal to ensure the outputs converge to the sliding mode surface. But the discontinuity of SMC may cause undesirable transient control performance, such as larger overshoot, longer settling time and stronger chattering. SMC with different structures has been already proposed to mitigate the effects of the above disadvantages, such as integral SMC,[14] fuzzy SMC,[15] backstepping SMC,[16] etc. However, these methods mainly improve the structure of SMC to reject lumped disturbances, which may induce serious control chattering. Recently, several reports about integrating SMC and disturbance observer had drawn the attention of researchers. In Song et al.[17] a multivariable high-order SMC with fixed-time extended state observer (ESO) approach was proposed to solve the attitude tracking problem for a quadrotor system with uncertain modelled exogenous disturbance and unknown parameters. In Rios et al.[18] a continuous SMC combined with sliding mode observer approach was proposed to design a robust controller for quadrotors, where the sliding mode observer is applied to reject the external disturbances and uncertainties. In Wang et al.[19] a real-time robust control scheme provided the efficient performance of a quadrotor using a disturbance-observer-based adaptive SMC method. It is necessary to highlight that the above works can provide a bounded tracking error for disturbances acting on the quadrotor dynamics, also ensuring the tracking error converges to zero. In the same vein, terminal SMC (TSMC) and its evolved versions have been known as one of the important techniques for achieving finite-time stability and giving rise to high steady-state tracking precision performance. For tracking control of a quadrotor, TSMC based on three kinds of disturbance observers was presented in Anwar and Malik.[20] However, the TSMC faces the singularity problem and has a slow convergence speed. To overcome these defects, an attitude control was developed for quadrotors using continuous nonsingular fast terminal SMC (NFTSMC) and ESO techniques,[21] which provides a bounded tracking error. A similar asymptotic tracking controller for a quadrotor was developed in Ke et al.[22] based on NFTSMC and high gain disturbance observer methods. Unlike the above works, this paper will integrate the advantages of both NFTSMC and LESO, which naturally breaks through their engineering application limitations. Different from general robust control methods, the proposed continuous nonsingular fast terminal sliding mode controller based on linear extended state observer (NFTSMC-LESO) provides an active approach to process disturbances, which can improve the robustness of the closed-loop system. Moreover, a continuous hyperbolic tangent function called Tanh is introduced to reduce the chattering, which has robustness to unbounded disturbances.[23]

Whether the aim is to design a robust controller or improve the design of a quadrotor system, a performance index must be selected and calculated. Then the system is treated as an optimized mathematical object since the control parameters are adjusted so that the index can reach an extremum value, commonly a minimum value. The best control performance is defined as the one that minimizes the index of controller. In this paper, we try to investigate a quantitative performance index that adequately represents the performance of the control system. Additionally, a self-adaptive fruit fly optimization algorithm (AFOA) is introduced to find the suboptimal or optimal control parameters. As one of the most important artificial intelligence algorithms, AFOA has the advantages of less parameters, easy implementation, fast calculation speed and strong ability of local search.[24] Meanwhile, the self-adaptive operator can help AFOA to jump out of local optimum.

Motivated by the above controller and observation, we have developed a robust attitude control strategy for a quadrotor. The main contributions of this paper are threefold. (1) The composition and the principle of the continuous NFTSMC-LESO are studied. More specially, a LESO is used to estimate and compensate the lumped disturbances. A continuous nonsingular fast terminal sliding mode surface is proposed to ensure the fast convergence to zero of the tracking error dynamics. (2) An improved fruit fly optimization algorithm is proposed to adjust the parameters of our controller. A self-adaptive operator is introduced to

help traditional algorithm jump out of local optimum. Then through step response test comparison and performance analysis, it is verified that the improved algorithm is feasible and effective. (3) The simulation and real application of the proposed controller are studied in attitude tracking control of an X450 quadrotor aircraft. The results prove that the proposed controller has better control performance and anti-interference ability. To the best of our knowledge, no reports on NFTSMC-LESO attitude control technique for quadrotor are available until now.

The outline of this paper is as follows. The attitude modelling of X450 quadrotor by the Euler–Lagrange method is described in 'Attitude dynamics' section. In 'LESO-based controller design' section, a robust control strategy and stability analysis are presented. Parameters tuning of the control system based on AFOA is illustrated in 'Parameters tuning based on AFOA' section. Three simulation cases are performed to demonstrate the effectiveness of the proposed controller in 'Numerical simulation' section. An experimental validation with flight tests is provided in 'Experimental results' section. Finally, some conclusions and contributions are summarized in 'Conclusion' section.

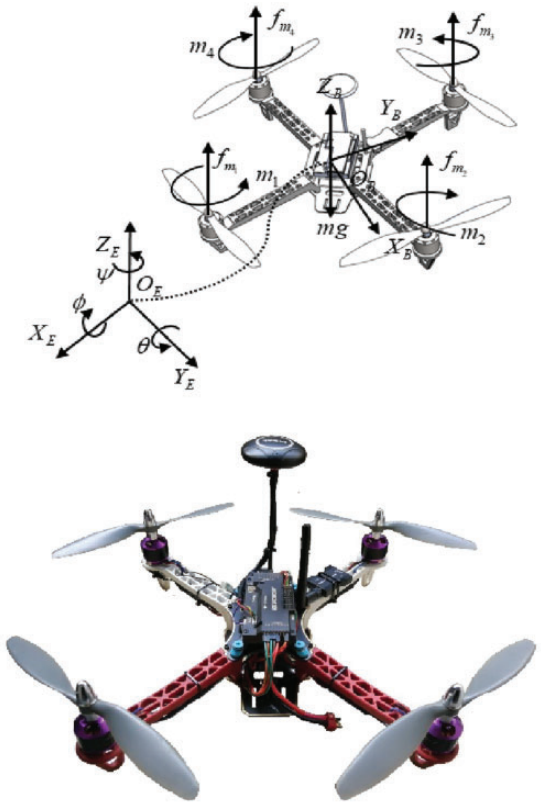

Figure 1. The reference frames and vectors of X450 quadrotor.

Attitude dynamics

The X450 quadrotor is actuated by the angular velocities of four electric motors as depicted in Figure 1. Define the thrust and torque produced by each motor as $f_{m_i}(i = 1, 2, 3, 4)$ and $m_i(i = 1, 2, 3, 4)$, respectively. The combination of the motors generates the main thrust U_1, the roll torque U_2, the pitch torque U_3 and the yaw torque U_4, which are described as

$$\begin{cases} U_1 = k_T(\Omega_1^2 + \Omega_2^2 + \Omega_3^2 + \Omega_4^2) = \sum_{i=1}^{4} f_{m_i} \\ U_2 = k_T(\Omega_2^2 - \Omega_4^2)l = (f_{m_2} - f_{m_4})l \\ U_3 = k_T(\Omega_3^2 - \Omega_1^2)l = (f_{m_3} - f_{m_1})l \\ U_4 = k_M(\Omega_2^2 + \Omega_4^2 - \Omega_1^2 - \Omega_3^2) \end{cases} \quad (1)$$

where $\Omega_i(i = 1, 2, 3, 4)$ is the angular velocity. f_{m_i} is calculated by the term $k_T\Omega_i^2$. m_i is equal to the term k_M multiplied by the square of the angular velocity. The identification process of k_T and k_M can be found in our previous work.[25]

The model of the attitude dynamics is obtained by Euler–Lagrange equations, which is expressed as[26]

$$\begin{cases} \ddot{\phi} = U_2/I_{xx} + \dot{\theta}\dot{\psi}(I_{yy} - I_{zz})/I_{xx} + d_1 \\ \ddot{\theta} = U_3/I_{yy} + \dot{\phi}\dot{\psi}(I_{zz} - I_{xx})/I_{yy} + d_2 \\ \ddot{\psi} = U_4/I_{zz} + \dot{\phi}\dot{\theta}(I_{xx} - I_{yy})/I_{zz} + d_3 \end{cases} \quad (2)$$

where (ϕ, θ, ψ) are the Euler angles (roll, pitch and yaw) and $d_i(i = 1, 2, 3)$ denotes the external disturbance.

Without loss of generality, the aforementioned external disturbance acting upon the quadrotor is chosen as crosswind,[27] as shown in Figure 2. A crosswind will occur perpendicular to the aircraft but parallel to the ground. The crosswind can overturn the aircraft or change the direction of forwarding motion. If the aircraft is disturbed by the crosswind, an additional force $f_{w_i}(i = 1, 2, 3, 4)$ acting over each rotor will be generated. In that case, the total thrust influenced by the crosswind is further described by

$$f_{T_i} = f_{m_i} + f_{w_i} = 2\rho A\hat{V}_i V_p \quad (3)$$

where $f_{T_i}(i = 1, 2, 3, 4)$ is the total thrust and V_p is the induced velocity of a propeller. $\hat{V}_i(i = 1, 2, 3, 4)$ is the total induced velocity, which is governed by

$$\hat{V}_i = \left[(V_{w_i}\cos\alpha + V_p)^2 + (V_{w_i}\sin\alpha)^2\right]^{1/2} \quad (4)$$

where α is the angle between the propeller axis and the direction of crosswind. For simplicity and obvious reasons for the aerodynamics, we choose $\alpha = 90^\circ$, i.e. the

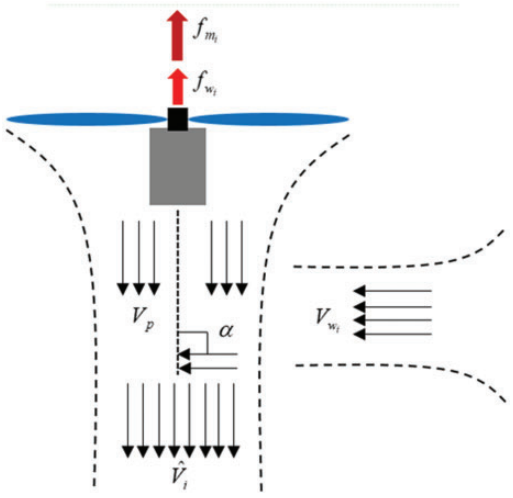

Figure 2. Mechanical analysis of the propeller under crosswind.

axis of wind is perpendicular to the Z-axis, and equation (4) becomes $\hat{V}_i = [{V_p}^2 + {V_{w_i}}^2]^{1/2}$. $V_{w_i}(i = 1, 2, 3, 4)$ denotes the crosswind velocity, which is a random variable.

Substituting (4) into (3), one gets

$$f_{w_i} = 2\rho A V_p^2 \left(1 + \frac{V_{w_i}^2}{V_p^2}\right)^{\frac{1}{2}} - f_{m_i} \tag{5}$$

In addition, the motor torque is opposed by aerodynamic drag, such that

$$m_{drag} = \rho A V_{w_i}^2 / 2 \tag{6}$$

Wind gusts acting on the aircraft adopt the form of torque. Hence, the detailed information of the wind gusts in (2) is given by

$$\begin{bmatrix} I_{xx} d_1 \\ I_{yy} d_2 \\ I_{zz} d_3 \end{bmatrix} = \begin{bmatrix} (f_{w_4} - f_{w_2}) l \\ (f_{w_3} - f_{w_1}) l \\ \sum_{i=1}^{4} m_{drag_i} \end{bmatrix} \tag{7}$$

Other physical parameters of the X450 quadrotor are listed in Table 1.

Table 1. Physical parameters of X450 quadrotor.

Parameter	Explanation	Value
l	Distance between the propeller and the centroid of X450	0.2 m
m	Mass of X450	1.923 kg
g	Gravitational acceleration constant	9.8 m/s^2
A	Propeller area	0.0113 m^2
ρ	Air density	1.29 kg/m^3
k_T	Thrust constant	1.45×10^{-6}
k_M	Torque constant	2.31×10^{-5}
I_{xx}	Rotational inertia around x-axis	0.094 kg $\cdot$ m^2
I_{yy}	Rotational inertia around y-axis	0.094 kg $\cdot$ m^2
I_{zz}	Rotational inertia around z-axis	0.086 kg $\cdot$ m^2

LESO-based controller design

Linear extended state observer

Equation (2) is recalled and rewritten as follows[28]

$$\begin{cases} \ddot{\phi} = b_2 U_2 + f_2(\phi, \dot{\phi}, \theta, \dot{\theta}, \psi, \dot{\psi}, w_2) \\ \ddot{\theta} = b_3 U_3 + f_3(\phi, \dot{\phi}, \theta, \dot{\theta}, \psi, \dot{\psi}, w_3) \\ \ddot{\psi} = b_4 U_4 + f_4(\phi, \dot{\phi}, \theta, \dot{\theta}, \psi, \dot{\psi}, w_4) \end{cases} \tag{8}$$

where w_i is the external disturbance and f_i is the uncertain function, also known as the lumped disturbance. Also $b_2 = 1/I_{xx}$, $b_3 = 1/I_{yy}$, $b_4 = 1/I_{zz}$.

Taking roll channel as an example, the controller design is developed as follows

$$\begin{cases} \dot{x}_1 = x_2 \\ \dot{x}_2 = f + bu \\ y = x_1 \end{cases} \tag{9}$$

where $x_1 = \phi$, $x_2 = \dot{\phi}$, f also represents the lumped disturbances, b is equal to b_2, u is equal to U_2.

System (9) in state-space form can be rewritten as

$$\begin{cases} \dot{\mathbf{x}} = \mathbf{A}\mathbf{x} + \mathbf{B}_1\mathbf{u} + \mathbf{B}_2\mathbf{f} \\ \mathbf{y} = \mathbf{C}\mathbf{x} \end{cases} \tag{10}$$

where $\mathbf{x} = [x_1, x_2]^T$, $\mathbf{u} = u$, $\mathbf{y} = [y_1, y_2]^T$, $\mathbf{f} = f$ are the state variable, control input, measured output and disturbances, respectively. $\mathbf{A} = \begin{bmatrix} 0 & 1 \\ 0 & 0 \end{bmatrix}$, $\mathbf{B}_1 = \begin{bmatrix} 0 \\ b \end{bmatrix}$, $\mathbf{B}_2 = \begin{bmatrix} 0 \\ 1 \end{bmatrix}$ and $\mathbf{C} = \begin{bmatrix} 1 & 0 \\ 0 & 1 \end{bmatrix}$ are given system matrices.

Remark 1. The lumped disturbance f is another form of the term $f(x, w(t), t)$, which contains parametric uncertainties, external disturbance and complex nonlinear dynamics.

Remark 2. System (10) represents a general class of system compared with (9) since the former is not confined to integral chained form, also may be subject to lumped disturbances.

Assumption 1. Assume that the lumped disturbance f is differentiable and bounded. It means $\|f\| < \infty$, $\|\dot{f}\| < \infty$ and their bounds are defined as $\sup_{t>0} \|f\| = f_b$, $\sup_{t>0} \|\dot{f}\| = h_b$.

An effective approach to estimate the lumped disturbances is to add an extended state term to the

observer. Specifically, (10) can be modified to the following form

$$\begin{cases} \dot{\bar{\mathbf{z}}} = \bar{\mathbf{A}}\bar{\mathbf{z}} + \bar{\mathbf{B}}\mathbf{u} + \mathbf{E}\mathbf{h} \\ \mathbf{y} = \bar{\mathbf{C}}\bar{\mathbf{z}} \end{cases} \tag{11}$$

where $\bar{\mathbf{z}} = [x_1, x_2, x_3]^T$, $\mathbf{h} = \dot{f}$, and $x_3 = f$ is the extended state. The system matrices $\bar{A}$, $\bar{B}$, $\bar{E}$ and $\bar{C}$ are designated as

$$\bar{\mathbf{A}} = \begin{bmatrix} 0 & 1 & 0 \\ 0 & 0 & 1 \\ 0 & 0 & 0 \end{bmatrix}, \quad \bar{\mathbf{B}} = \begin{bmatrix} 0 \\ b \\ 0 \end{bmatrix}, \quad \mathbf{E} = \begin{bmatrix} 0 \\ 0 \\ 1 \end{bmatrix}, \quad \bar{\mathbf{C}} = [1 \quad 0 \quad 0] \tag{12}$$

Let the LESO for (11) be defined as follows

$$\begin{cases} \dot{\hat{\bar{\mathbf{z}}}} = \bar{\mathbf{A}}\hat{\bar{\mathbf{z}}} + \bar{\mathbf{B}}\mathbf{u} + \mathbf{L}(\mathbf{y} - \hat{\mathbf{y}}) \\ \hat{\mathbf{y}} = \bar{\mathbf{C}}\hat{\bar{\mathbf{z}}} \end{cases} \tag{13}$$

where $\hat{\bar{\mathbf{z}}} = [\hat{x}_1, \hat{x}_2, \hat{x}_3]^T$ is an estimation of the state variable $\bar{\mathbf{z}}$. Matrix $\mathbf{L}$ is the observer gain, which can be obtained by a pole placement method[29]

$$\mathbf{L} = \begin{bmatrix} l_1 \\ l_2 \\ l_3 \end{bmatrix} = \begin{bmatrix} \varsigma_1\omega_o \\ \varsigma_2\omega_o^2 \\ \varsigma_3\omega_o^3 \end{bmatrix} \tag{14}$$

where $\omega_o > 0$ is the so-called observer bandwidth. $\varsigma_i (i = 1, 2, 3)$ is chosen such that $\lambda(s) = s^3 + \varsigma_1 s^2 + \varsigma_2 s + \varsigma_3$ is Hurwitz. And ς_i satisfies

$$\varsigma_i = \frac{3!}{i!(3-i)!}, \; i = 1, 2, 3 \tag{15}$$

Define the estimation error of LESO as

$$\mathbf{e}_{\bar{z}} = \bar{\mathbf{z}} - \hat{\bar{\mathbf{z}}} \tag{16}$$

Subtracting (13) from (11), one gets

$$\dot{\mathbf{e}}_{\bar{z}} = (\bar{\mathbf{A}} - \mathbf{L}\bar{\mathbf{C}})\mathbf{e}_{\bar{z}} - \mathbf{E}\mathbf{h} = \mathbf{A}_e - \mathbf{E}\mathbf{h} \tag{17}$$

where $\mathbf{A}_e = \begin{bmatrix} -\varsigma_1\omega_o & 1 & 0 \\ -\varsigma_2\omega_o^2 & 0 & 1 \\ -\varsigma_3\omega_o^3 & 0 & 0 \end{bmatrix}$.

Assumption 2. The estimation error in (16) is bounded, and it satisfies $\mathbf{e}_{\bar{z}}^* = \sup_{t>0} |\mathbf{e}_{\bar{z}}(t)|$.

Remark 3. The LESO is bounded input and bounded output and all the eigenvalues $\lambda(s)$ of $\mathbf{A}_e$ are in the left half plane. An appropriate observer gain L is chosen to ensure $\mathbf{A}_e$ Hurwitz under Assumption 1.

Remark 4. Assume the derivative of lumped disturbance $\dot{f}$ in (10) satisfies the condition $\lim_{t\to\infty} \|\dot{f}\| = 0$, the estimation error will approach zero asymptotically.

Proof. For any eigenvalue $\lambda_i < \lambda_j (i < j$, and $i, j = 1, 2, 3)$, one obtains

$$|\lambda\mathbf{I}_3 - \mathbf{A}_e| = \prod_{i=1}^{3}(\lambda + \lambda_i) \tag{18}$$

From (17), we know that $\mathbf{A}_e$ has three unique eigenvalues. Therefore, there exists an invertible real matrix T that satisfies

$$\mathbf{A}_e = \mathbf{T}diag(-\lambda_1, -\lambda_2, -\lambda_3)\mathbf{T}^{-1} \tag{19}$$

By using the exponential form, (19) can be rewritten as

$$e^{\mathbf{A}_e t} = \mathbf{T}diag(e^{-\lambda_1 t}, e^{-\lambda_2 t}, e^{-\lambda_3 t})\mathbf{T}^{-1} \tag{20}$$

For any $t > 0$, it follows that

$$\|e^{\mathbf{A}_e t}\|_{m_\infty} \le \beta h_b e^{-\lambda_1 t} \tag{21}$$

where β is a weight function. It should be noticed that m_∞ norm of a square matrix is equal to the product of its order value and maximum element.

Solution of the error in (17) is calculated as

$$\mathbf{e}_{\bar{z}}(t) = e^{\mathbf{A}_e t}\mathbf{e}_{\bar{z}}(0) + \int_0^t e^{\mathbf{A}_e(t-\tau)}\mathbf{E}\mathbf{h}(\tau)\mathrm{d}\tau \tag{22}$$

Obviously, the error is state-stable with Assumption 1. Moreover, according to the compatibility between m_∞ norm and vector norm of a complex field, one gets

$$\begin{aligned} \|\mathbf{e}_{\bar{z}}(t)\| &\le \|e^{\mathbf{A}_e t}\|\|\mathbf{e}_{\bar{z}}(0)\| + \left\| \int_0^t e^{\mathbf{A}_e(t-\tau)}\mathbf{E}\mathbf{h}(\tau)\mathrm{d}\tau \right\| \\ &\le \|e^{\mathbf{A}_e t}\|_{m_\infty}\|\mathbf{e}_{\bar{z}}(0)\| \\ &\quad + \int_0^t \|e^{\mathbf{A}_e(t-\tau)}\|_{m_\infty}\|\mathbf{E}\|\|\mathbf{h}(\tau)\|\mathrm{d}\tau \\ &\le \beta h_b e^{-\lambda_1 t}\|\mathbf{e}_{\bar{z}}(0)\| + \int_0^t \beta h_b e^{-\lambda_1(t-\tau)}\mathrm{d}\tau \\ &\le \beta h_b e^{-\lambda_1 t}\|\mathbf{e}_{\bar{z}}(0)\| + \frac{\beta h_b}{\lambda_1}(1 - e^{-\lambda_1 t}) \end{aligned} \tag{23}$$

where $\mathbf{e}_{\bar{z}}(0)$ is the initial condition. Since $\lim_{t\to\infty} e^{-\lambda_1 t} = 0$, the system asymptotically reaches

$$\|\mathbf{e}_{\bar{z}}(t)\| \le \frac{\beta h_b}{\lambda_1} \tag{24}$$

Remark 5. Assume the first derivative of lumped disturbance satisfies $\lim_{t\to\infty}\|\dot{f}\| = \lim_{t\to\infty} h_b = 0$, the estimation error will tend to zero asymptotically, i.e. $\lim_{t\to\infty}\|\mathbf{e}\bar{z}(t)\| = 0$.

Design of NFTSMC-LESO control law

SMC is deemed as one of the important nonlinear control techniques with the ability to process the coupling disturbances and strong nonlinearities.[30] It can be divided into two subparts: the design of a stable sliding mode surface and the design of a control law to compel the system states into the chosen surface.

Consider a continuous NFTSM surface defined as[31]

$$s = e + \beta|\dot{e}|^{\gamma}\tanh(\dot{e}) = e + \beta\mathrm{sig}(\dot{e})^{\gamma} = 0 \tag{25}$$

where $\beta > 0$, $1 < \gamma < 2$. The tracking error e is equal to x_r minus $\hat{x}_1$. The first derivative $\dot{e}$ is equal to $\dot{x}_r$ minus $\hat{x}_2$. x_r and $\dot{x}_r$ are the referenced signal and its first derivative, respectively.

Remark 6. In (25), we use the hyperbolic tangent function Tanh to approximate the Signum function, for avoiding the chattering.

Lemma 1. The first derivative of (25) can be calculated as $\dot{s} = \dot{e} + \beta\gamma|\dot{e}|^{\gamma-1}\ddot{e}$ although the Tanh operator and absolute value are involved.

Proof. The proof process of Lemma 1 can be found in Yu et al.[28]

Substituting the first derivative of (24) into (8), one obtains an equivalent input

$$u_e = b^{-1}[\beta^{-1}\gamma^{-1}sig(\dot{e})^{2-\gamma} + \ddot{x}_r - \hat{x}_3] \tag{26}$$

where $\ddot{x}_r$ is the second derivative of the referenced signal.

To ease chattering and reconcile the need for fast finite-time convergence, we design a fast terminal sliding mode type as the reaching law[32]

$$\dot{s} = -k_1 s - k_2\mathrm{sig}(s)^{p} \tag{27}$$

where $0 < p < 1$ and k_1 and k_2 are constant.

Then, the reaching input is defined as

$$u_r = b^{-1}(k_1 s + k_2\mathrm{sig}(s)^{p}) \tag{28}$$

Hence, the NFTSMC-LESO is obtained by combining the equivalent input and reaching input

$$u = u_e + u_r \tag{29}$$

Stability analysis for NFTSMC

Lemma 2. For a Lyapunov function, it satisfies the following inequality

$$\dot{V} + \xi V + \rho V^{\delta} \le 0 \tag{30}$$

where $\xi,\rho > 0$, then the settling time is described as

$$T_s \le \xi^{-1}(1-\delta)^{-1}\ln(1 + \xi\rho^{-1}V_0^{1-\delta}) \tag{31}$$

where V_0 is the initial value.

The proof process of Lemma 2 can be found in Nekoukar and Erfanian.[33]

Consider the Lyapunov function

$$V = \frac{1}{2}s^{T}s \tag{32}$$

and its first derivative is

$$\dot{V} = s^{T}\dot{s} \tag{33}$$

Combining (29) and (9), the first derivative of the proposed sliding mode surface is rewritten as

$$\begin{aligned}\dot{s} = \dot{e} + \beta\gamma|\dot{e}|^{\gamma-1}(&\beta^{-1}\gamma^{-1}sig(\dot{e})^{2-\gamma}\\ &-k_1 s - k_2\mathrm{sig}(s)^{p} + \hat{x}_3 - f)\end{aligned} \tag{34}$$

Then

$$\dot{V} = \beta\gamma|\dot{e}|^{\gamma-1}(\hat{x}_3 - f) - \bar{k}_1 s^2 - \bar{k}_2\mathrm{sig}(s)^{p+1} \tag{35}$$

where $\bar{k}_i = \beta\gamma|\dot{e}|^{\gamma-1}k_i (i = 1, 2)$.

Equation (33) can also be described as the following forms

$$\dot{V} = -\left[\bar{k}_1 - \beta\gamma|\dot{e}|^{\gamma-1}(\hat{x}_3 - f)s^{-1}\right]s^2 - \bar{k}_2|s|^{p+1} \tag{36}$$

$$\dot{V} = -\bar{k}_1 s^2 - [\bar{k}_2 - \beta\gamma|\dot{e}|^{\gamma-1}(\hat{x}_3 - f)sig(s)^{-p}]|s|^{p+1} \tag{37}$$

For (36), if $\bar{k}_1 - \beta\gamma|\dot{e}|^{\gamma-1}(\hat{x}_3 - f)s^{-1}$ is positive definite, then the finite time stability of the sliding mode surface is guaranteed

$$\|s\| \le |\beta\gamma|\dot{e}|^{\gamma-1}(\hat{x}_3 - f)|/\bar{k}_1 = |\hat{x}_3 - f|/\bar{k}_1 = \Delta_1 \tag{38}$$

Similarly, if $\bar{k}_2 - \beta\gamma|\dot{e}|^{\gamma-1}(\hat{x}_3 - f)sig(s)^{-p}$ is positive, the analysis of (37) is given by

$$\|s\| \le [|\beta\gamma|\dot{e}|^{\gamma-1}(\hat{x}_3 - f)|/\bar{k}_2]^{1/p} = (|\hat{x}_3 - f|/\bar{k}_2)^{1/p} = \Delta_2 \tag{39}$$

According to the feature of (37) and (38), the sliding mode surface can converge into the following region in finite time

$$\|s\| \le \Delta = \min(\Delta_1, \Delta_2) \tag{40}$$

Since $\|s\| \le \Delta$, the NFTSM surface in (24) can be rewritten as

$$e + \left(\beta - \frac{s}{\text{sig}(\dot{e})^{\gamma}}\right)\text{sig}(\dot{e})^{\gamma} = 0 \tag{41}$$

when $\beta - \frac{s}{\text{sig}(\dot{e})^{\gamma}}$ is positive, (41) holds the form of NFTSM. And the first derivative of tracking error converges into the region

$$|\dot{e}| \le (\Delta/\beta)^{1/\gamma} \tag{42}$$

in finite time. Combining (41) and (42) yields

$$|e| \le \beta|\dot{e}|^{\gamma} + |s| \le 2\Delta \tag{43}$$

the tracking error will converge into the region in finite time.

This implies that the system state will slide to the desired equilibrium area asymptotically under the proposed control law NFTSMC-LESO.

Remark 7. Equations (28) and (40), once the larger parameters k_1 and k_2 are selected, the smaller boundary Δ will be obtained. However, it will also cause saturation of actuators and damage to the components in the system.

Parameters tuning based on AFOA

Basic principle of FOA

FOA is a swarm intelligence optimization algorithm firstly proposed by Pan et al.,[34] which can obtain global optimization using the food search mechanism of the fruit fly. During the searching process, the fruit flies search for food sources in several points and fly toward the point according to greatest odour intensity. Then the rest of fruit flies swarm are called upon to fly towards the point. The detailed steps of FOA are described as follows:

1. *Parameter initialization*. Initial the group size G_s, maximum iteration $T_{\max}$ and swarm location range (X_{axis}, Y_{axis}).
2. *Stochastic distance calculation*. Give stochastic distance and direction to individual fruit fly for finding food through the smell

$$\begin{cases} X_i = X_{axis} + SV \\ Y_i = Y_{axis} + SV \end{cases} \tag{44}$$

3. *Odour intensity calculation*. Since the food location is unknown, the distance between the original location and fruit fly is estimated with an evaluation index of the odour intensity

$$\begin{cases} Dist_i = \sqrt{X_i^2 + Y_i^2} \\ E_i = 1/Dist_i \end{cases} \tag{45}$$

4. *Objective function calculation*. Substitute evaluation index E_i into an objective function to calculate the odour intensity of the individual location of a fruit fly. Moreover, the best individual with maximal odour intensity will be found out

$$\begin{cases} Smell_i = \text{Function}(E_i) \\ [BestSmell \quad BestIndex] = max(Smell) \end{cases} \tag{46}$$

5. *Population evolution*. Keep maximal odour intensity and X, Y coordinates, all the fruit flies will fly towards this location

$$\begin{cases} Smellbest = bestSmell \\ X_{axis} = X(BestIndex) \\ Y_{axis} = Y(BestIndex) \end{cases} \tag{47}$$

6. *Termination criterion*. FOA will stop when the maximum iteration is reached. Otherwise, the algorithm repeats Steps (2) to (5) and judge whether the odour intensity is higher than that in the previous iteration. If yes, implement Step (6).

Self-adaptive operator

The step size in traditional FOA is fixed, which may be trapped into local optimum.[35] The convergence rate and iteration precision depend on the step size. Hence, a self-adaptive operator is introduced to provide a variable step size for FOA, which is given by

$$h_i = \frac{\omega_m}{BestSmell_{i-1}} e^{-\tau \cdot \left(\frac{T}{T_{\max}}\right)^{\mu}} + h_{\min} \tag{48}$$

where $\omega_m \in (0, 1)$ is an adjustment factor, $BestSmell_{i-1}$ is the optimal odour intensity in the last iteration, $\tau \in (0, 1)$ is a limited factor, T is the current iteration, $h_{\min}$ is the minimal step size and μ is a positive constant.

Furthermore, (44) can be rewritten as

$$\begin{cases} X_i = X_{axis} + h_i \cdot (2 \cdot rand - 1) \\ Y_i = Y_{axis} + h_i \cdot (2 \cdot rand - 1) \end{cases} \tag{49}$$

where rand is a random constant between 0 and 1.

With the self-adaptive operator, AFOA has a large random step size at the early iteration to avoid premature convergence. At the subsequent iteration, small step size will enhance its local optimization ability.

Numerical simulation

In this section, evaluation of the proposed controller NFTSMC-LESO is presented through three cases. The Simulink model is established using the nonlinear model of a quadrotor defined in (2). And the proposed controller is applied on the aircraft to check the control performance.

Case 1: *Parameters tuning*. A performance index is a mathematical quantitative measure of the control performance. In this case, we select a performance index called integral of time multiplied by the squared error (ITSE) as the objective function of the AFOA, which is proposed in Rene and Marta[36] and given as follows

$$F_c = \int_0^T t(e(t))^2 \mathrm{d}t \tag{50}$$

where $e(t)$ is tracking error in the time domain. The upper limit T is chosen as a finite time so that the integral reaches a steady-state.

Remark 8. In the NFTSMC-LESO (29), the initial conditions are set as $\gamma = 1.5$, $p = 0.5$. Therefore, only 12 control parameters will be adjusted by the AFOA.

As a standard test input signal, the step signal $\Theta_r = [1 \quad -1 \quad 0.5]$rad is chosen as the referenced command, and the initial attitude angles and attitude velocities are set to 0 rad and 0 rad/s. Meanwhile, the parameters of AFOA are set as follows: $G_s = 20$, $T_{\max} = 100$, $\omega_m = 0.8$, $\tau = 0.2$, $\mu = 10$, $h_{\min} = 1$. For comparisons, the controller is also adjusted by improved genetic algorithm (IGA)[37] and FOA. Wind gusts simulated using (7) are added to the attitude dynamics of quadrotor. The variables V_{w_i} and V_p are selected as random sequences. Figures 3 to 7 portray the results of Case 1. The cost values in Figure 3 are normalized with the objective functions. The minimum cost value of AFOA is 0.002, which is 14.3% of that from FOA (0.014), and 40% of that from IGA (0.005). It can be summarized that AFOA is superior to FOA and IGA. It can also be observed that the searching process with ITSE index has an ability of in-depth data mining, and the AFOA can help NFTSMC-LESO to obtain a desired tracking performance, as shown in Figure 5. Furthermore, the so-called lumped disturbances, wind gusts are accurately estimated by LESO, as shown in Figure 4. Figures 6 and 7 also give the responses of angular velocities and control laws. The optimal control parameters adjusted by ITSE index are listed in Table 2. The role of Case 1 is to provide a set of probable control parameters for manual tuning in the real application.

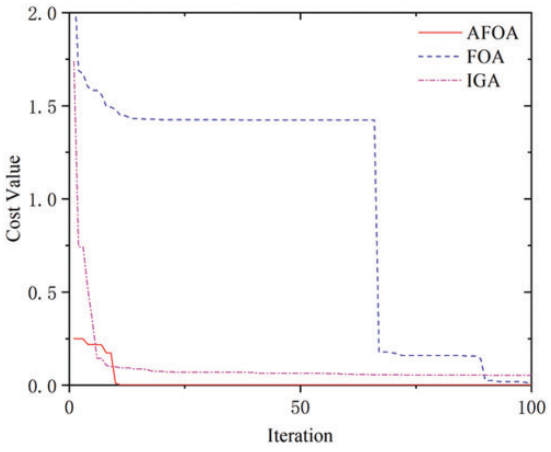

Figure 3. Iteration curves.
AFOA: adaptive fruit fly optimization algorithm; IGA: improved genetic algorithm.

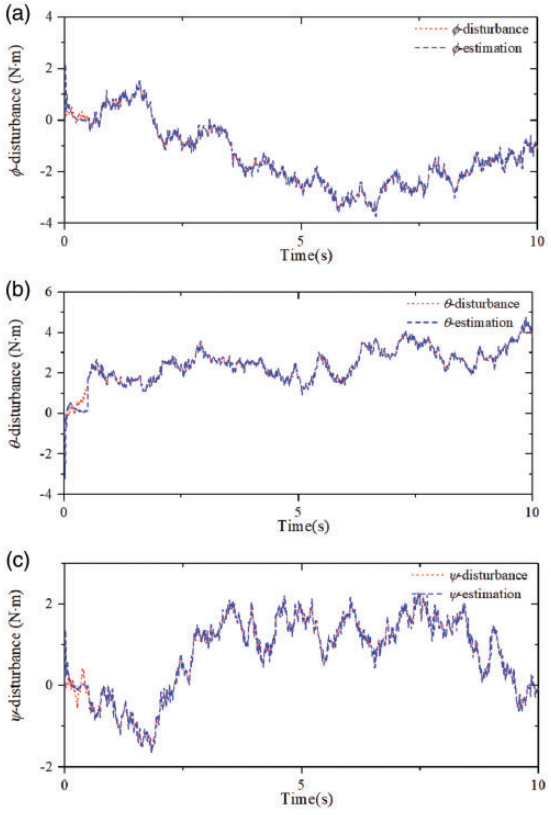

Figure 4. Disturbances and their estimation: (a) roll loop; (b) pitch loop; (c) yaw loop.

Case 2: *Anti-disturbance analysis*. The goal of this case is to compare the ability of anti-disturbance

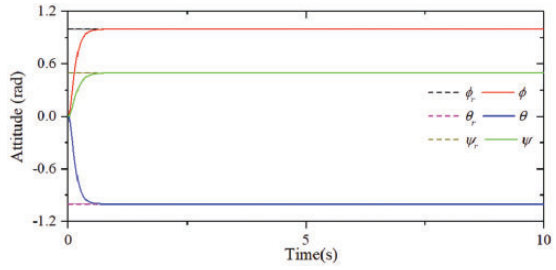

Figure 5. Attitude response.

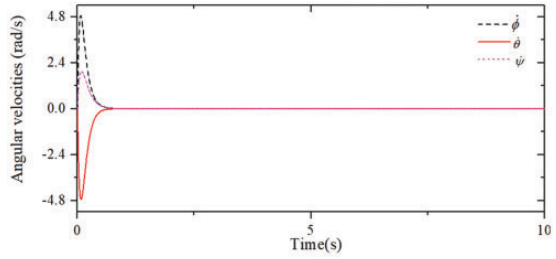

Figure 6. Angular velocities response.

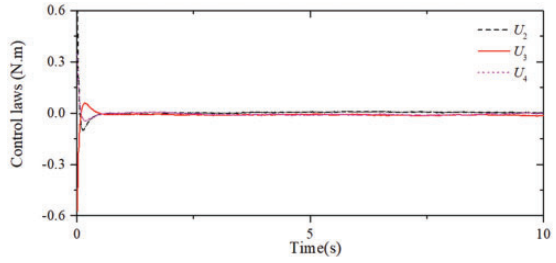

Figure 7. Attitude control laws.

between the LESO and ESO in the presence of variable disturbances. Taking the pitch angle as an example, we still choose the step signal as the referenced command. All control parameters are the same as those provided in Case 1. The structure and control parameters of the ESO are given in Appendix 1. The coefficient of correlation provides an effective measure of observer robustness, and reflects observer sensitivity or correlation between disturbances. The robustness index is given by

$$\text{Robustness} = \frac{\sum_{i=1}^{N}(f_i-\bar{f})(\hat{f}_i-\bar{\hat{f}})}{\sqrt{\sum_{i=1}^{N}(f_i-\bar{f})^2\sum_{i=1}^{N}(\hat{f}_i-\bar{\hat{f}})^2}} \times 100\% \tag{51}$$

where $\bar{f}$ is the mean value of the lumped disturbance f_i, and $\bar{\hat{f}}$ is the mean value of the disturbance estimation $\hat{f}_i$. The bigger the robustness value, the stronger the ability of disturbance rejection will be.

Table 2. Optimal control parameters using ITSE index.

Parameter	Value	Parameter	Value
$\omega_{o-\phi}$	506.11	$k_{1-\theta}$	436.01
β_{ϕ}	0.06	$k_{2-\theta}$	275.85
$k_{1-\phi}$	688.53	$\omega_{o-\psi}$	497.07
$k_{2-\phi}$	151.88	β_{ψ}	0.01
$\omega_{o-\theta}$	485.48	$k_{1-\psi}$	324.63
β_{θ}	0.02	$k_{2-\psi}$	105.32

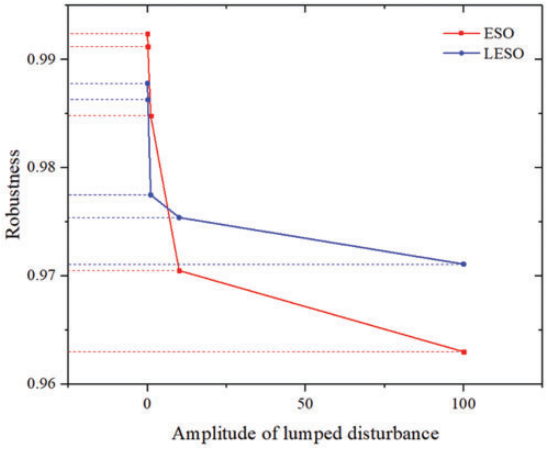

Figure 8. Robustness of ESO and LESO.
ESO: extended state observer; LESO: linear extended state observer.

In this case, wind gusts with different amplitudes are considered to test the ability of anti-disturbance of the two observers. The simulation runs for 10 s, and the results are shown in Figure 8. As a result, the robustness values of the observers will decrease with the increased amplitude of the lumped disturbance. When the amplitude belongs to the interval [0.01,1], the robustness of ESO is stronger than that of LESO. Alternatively, the robustness of LESO becomes stronger than that of ESO when the amplitude belongs to the interval [10,100]. Hence, the LESO is more suitable for dealing with big amplitude of disturbances; a similar conclusion can be found in Li et al.[38]

Case 3: *Performance comparison*. The workability of the NFTSMC-LESO compared to two other controllers named SMC based on LESO (SMC-LESO) and linear active disturbance rejection control (LADRC) are discussed in this case. The parameters of the two controllers are listed in Appendix 2, which are also adjusted by AFOA. Control parameters of NFTSMC-LESO are the same as those provided in the previous case. We employ the wind gusts described in Case 1 into the closed-loop system to show the performance of those controllers under disturbances, but

the amplitude of the disturbances increases 10 times. Take the roll angle as an example, and the referenced signal is defined as

$$\phi_r = \begin{cases} 0, t \in [0, 5) \\ 0.1\cos(0.25\pi t - 1.25\pi), t \in [5, 10] \end{cases} \quad (52)$$

the results are depicted in Figures 9 and 10. The responses of roll angle have the same trend as the referenced signal based on the three controllers in Figure 9. From the enlarged graph, it is clear that NFTSMC-LESO has a better performance in response speed and trajectory precision than the other controllers when the referenced signal has a drastic change. Figure 10 shows the input signals, from which it can be seen that the developed approach has a smoother control curve and can avoid the chattering effectively.

To further analyze the tracking performance intuitively and precisely, Table 3 presents a set of statistical indicators which includes root mean square error (RMSE), maximum error (ME), mean error (MeanE) and robustness. The RMSE value of NFTSMC-LESO is 66.67% and 81.16% of those of SMC-LESO and LADRC, respectively. Similar results can be calculated with ME and MeanE. It is obvious that the trajectory precision of NFTSMC-LESO is higher than that of the other two controllers. Additionally, the observer bandwidth ω_o is sensitive to the noise and sampling rate. The larger the observer bandwidth, the sooner the disturbance is observed, but the bigger initial overshoot is also generated, as concluded in Yu et al.[28] Big overshoot will cause the decline of the robustness. In the process of parameters tuning, only the tracking error rather than robustness is chosen as the performance index. According to the table, the robustness value of NFTSMC-LESO is slightly weaker compared to LADRC, which may be acceptable for attitude control. The result shows that the proposed controller has a relatively superior control performance under lumped disturbances.

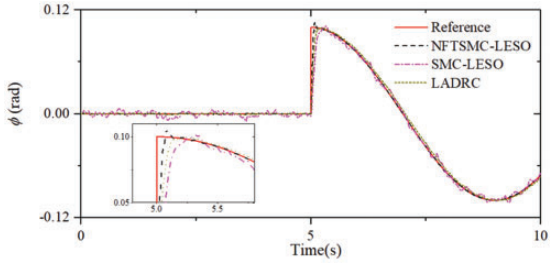

Figure 9. Roll angle response.
LADRC: linear active disturbance rejection control; NFTSMC-LESO: nonsingular fast terminal sliding mode control based on linear extended state observer; SMC-LESO: sliding mode control-linear extended state observer.

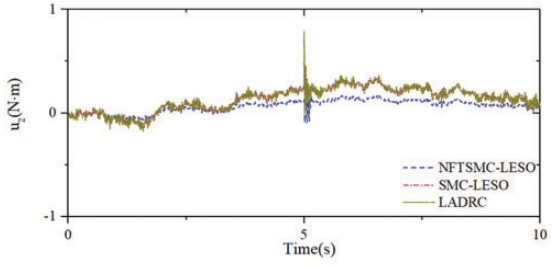

Figure 10. Input of roll channel.
LADRC: linear active disturbance rejection control; NFTSMC-LESO: nonsingular fast terminal sliding mode control based on linear extended state observer; SMC-LESO: sliding mode control-linear extended state observer.

Table 3. Performance comparison of controllers.

Controller	NFTSMC-LESO	SMC-LESO	LADRC
RMSE	0.0056	0.0084	0.0069
ME	0.1006	0.1027	0.1005
MeanE	0.0002	0.0011	0.0007
Robustness	98.5372%	96.9951%	99.1008%

LADRC: linear active disturbance rejection control; ME: maximum error; MeanE: mean error; NFTSMC-LESO: nonsingular fast terminal sliding mode control based on linear extended state observer; RMSE: root mean square error; SMC-LESO: sliding mode control-linear extended state observer.

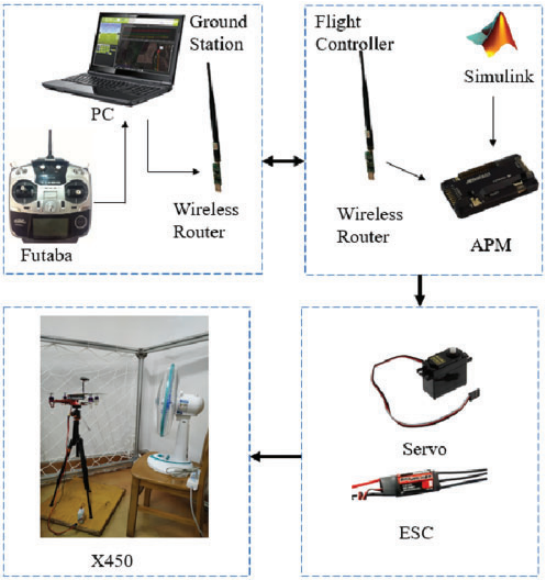

Figure 11. X450 quadrotor experimental platform.
APM: Auto Pilot Mega.

Experimental results

The proposed controller is tested on an X450 quadrotor experimental platform depicted in Figure 11. The platform contains an X450 quadrotor, two wireless routers, a ground station, an open-source flight control module called Auto Pilot Mega (APM) and a Futaba remote control unit. The APM is employed to generate the commands to control the angular speeds of four propellers. An inertial measurement unit installed on the APM is used to measure attitude angles and angular speeds. The quadrotor communicates with the ground station via a pair of wireless routers at a frequency of 50 Hz. Before the experiment, the control algorithms are embedded into the APM directly from Matlab/Simulink through a plug-in called APM2 Simulink Blockset.[39] It is pointed out that the GPS module is not used in the experiment for closed-loop attitude control.

The quadrotor is installed on a universal joint bracket with a negative 70° initial angle. The connection restricts the translational motion of the aircraft. During the experiment, a pilot operates the aircraft flying in hover by Futaba controller. Then, the Futaba is switched into the automatic flight mode for desired trajectories tracking using NFTSMC-LESO. Lastly, the hovering operation is activated again to keep the quadrotor from striking the bracket. Three kinds of wind gusts with fixed speeds are added into the experiments through an electric fan. And the initial angle of the fan is 90°, i.e. the central line of the fan is perpendicular to the central line of the propeller hub of quadrotor when the aircraft flies in hovering. We select three kinds of referenced trajectories for attitude tracking control experiments. To show the efficiency of the proposed controller, a comparison between NFTSMC-LESO with SMC-LESO, and LADRC is performed. The collected experimental data lasts 10 s, and the results are shown in Figures 12 to 17. It can be observed from Figures 12 to 14 that all the three controllers can make the attitude angles track the referenced trajectories in spite of mechanical vibration and unmeasured wind gusts. Since all three controllers use the same DOB technology, the results demonstrate that the attitude responses obtained by NFTSMC-LESO ensure faster convergence and higher precision than the other controllers. As the wind speed increases, the proposed controller still performs good tracking performance and robustness.

Furthermore, the attitude tracking error described by RMSE is presented in Table 4 to evaluate the three controllers. For roll angle, the RMSE value of NFTSMC-LESO is 35.37% and 54.12% than those of SMC-LESO and LADRC, respectively. For pitch angle, the percentages are 47.25% and 55.19%, respectively. For the yaw angle, the percentages are 46.81% and 52.55%, respectively. It is obvious that the quadrotor equipped with NFTSMC-LESO controller tracks the desired commands with higher precision. These results also verify the conclusions given in 'Numerical simulation' section.

The input torques of the three controllers are depicted in Figures 15 to 17. From the results, it can

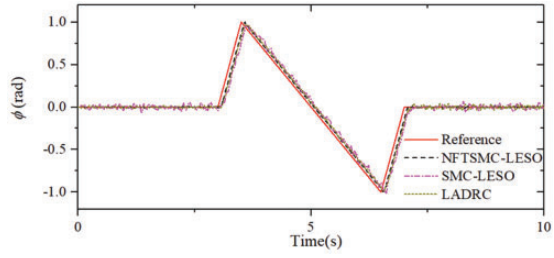

Figure 12. The tested roll angle response when $V_w = 1.25$ m/s.
LADRC: linear active disturbance rejection control; NFTSMC-LESO: nonsingular fast terminal sliding mode control based on linear extended state observer; SMC-LESO: sliding mode control-linear extended state observer.

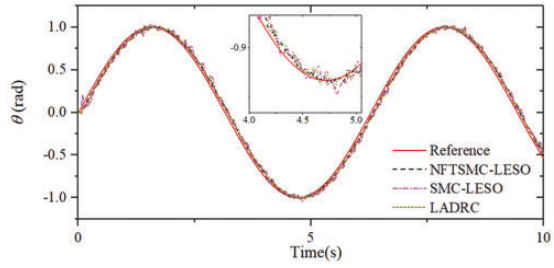

Figure 13. The tested pitch angle response when $V_w = 2.75$ m/s.
LADRC: linear active disturbance rejection control; NFTSMC-LESO: nonsingular fast terminal sliding mode control based on linear extended state observer; SMC-LESO: sliding mode control-linear extended state observer.

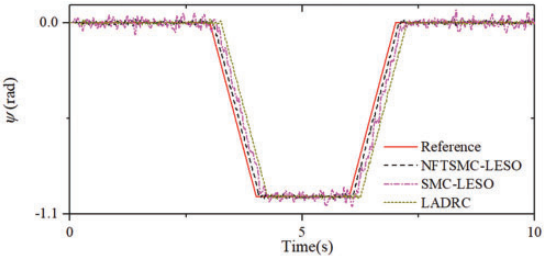

Figure 14. The tested yaw angle response when $V_w = 3.75$ m/s.
LADRC: linear active disturbance rejection control; NFTSMC-LESO: nonsingular fast terminal sliding mode control based on linear extended state observer; SMC-LESO: sliding mode control-linear extended state observer.

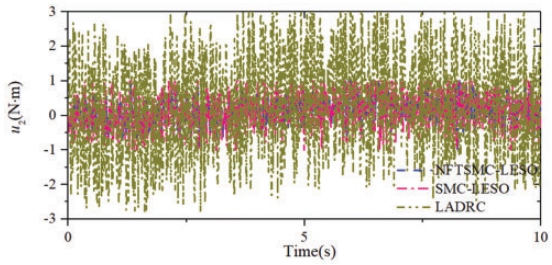

Figure 15. The response of roll torque.
LADRC: linear active disturbance rejection control; NFTSMC-LESO: nonsingular fast terminal sliding mode control based on linear extended state observer; SMC-LESO: sliding mode control-linear extended state observer.

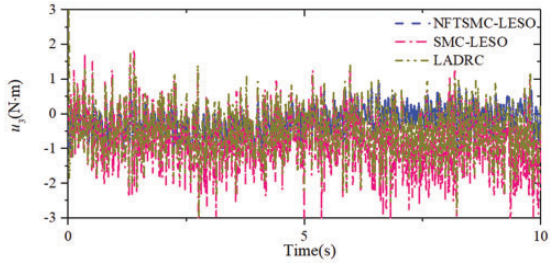

Figure 16. The response of pitch torque.
LADRC: linear active disturbance rejection control; NFTSMC-LESO: nonsingular fast terminal sliding mode control based on linear extended state observer; SMC-LESO: sliding mode control-linear extended state observer.

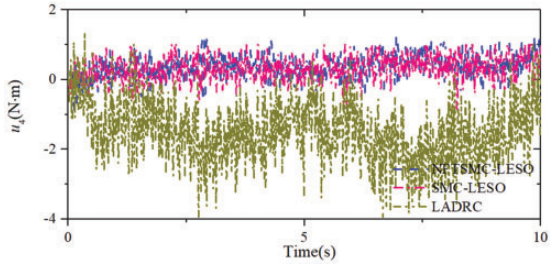

Figure 17. The response of pitch torque.
LADRC: linear active disturbance rejection control; NFTSMC-LESO: nonsingular fast terminal sliding mode control based on linear extended state observer; SMC-LESO: sliding mode control-linear extended state observer.

be observed that NFTSMC-LESO requires smaller rotational torques than the other two controllers. This implies that both disturbances and chattering have been significantly reduced by the proposed controller. In addition, from Figures 15 and 17, LADRC requires larger rotational torques to reject the lumped disturbances when the aircraft tracks non-smooth trajectories. This implies that the SMC structures of NFTSMC-LESO and SMC-LESO are superior to the control structure of LADRC.

Table 4. RMSE of the three controllers.

RMSE	ϕ	θ	ψ
NFTSMC-LESO	0.0197	0.0266	0.0330
SMC-LESO	0.0557	0.0563	0.0705
LADRC	0.0364	0.0482	0.0628

LADRC: linear active disturbance rejection control; NFTSMC-LESO: nonsingular fast terminal sliding mode control based on linear extended state observer; RMSE: root mean square error; SMC-LESO: sliding mode control-linear extended state observer.

Conclusion

In this paper, a novel NFTSMC-LESO controller is designed and investigated for the attitude tracking control of a quadrotor. The new controller is model-free and can guarantee rapid convergence rate and high accuracy control performance subjected to lumped disturbances. Stability of the closed-loop system is analyzed based on Lyapunov function. Simulation cases and experiments are conducted to demonstrate the effectiveness of our proposed controller. Some results are summarized into the following points: (1) The proposed controller can ensure a satisfactory attitude tracking control performance both in simulations and experiments. (2) For parameters tuning, AFOA based on ITSE index can obtain a set of optimal control parameters for NFTSMC-LESO controller. (3) Compared with ESO, the LESO is more suitable for dealing with big amplitude of disturbances. (4) Under lumped disturbances, the proposed controller performs a better control than the existing SMC-LESO and LADRC.

In future, we will use the NFTSMC-LESO method to design the position tracking control for the quadrotor. Furthermore, outdoor flight experiments will be carried out to test the performance of the control technology in the presence of real wind gusts.

Declaration of conflicting interests

The author(s) declared no potential conflicts of interest with respect to the research, authorship, and/or publication of this article.

Funding

The author(s) disclosed receipt of the following financial support for the research, authorship, and/or publication of this article: This work was supported by the National Natural Science Foundation of China under Grant No. 5180522, the Foundation Research Project of Jiangsu Province under Grant No. BK20170315.

ORCID iD

Li Ding https://orcid.org/0000-0002-3613-134X

References

1. Ghommam J and Saad M. Autonomous landing of a quadrotor on a moving platform. *IEEE Trans Aerosp Electron Syst 2017; 53: 1504–1519*.
2. Liang X, Fang YC, Sun N, et al. Nonlinear hierarchical control for unmanned quadrotor transportation systems. *IEEE Trans Ind Electron 2018; 65: 3395–3405*.
3. Kougianos E, Mohanty SP, Coelho G, et al. Design of a high-performance system for secure image communication in the internet of things. *IEEE Access 2016; 4: 1222–1242*.
4. Ru PK and Subbarao K. Nonlinear model predictive control for unmanned aerial vehicles. *Aerospace 2017; 4:31*.
5. Tran T, Ge SS and He W. Adaptive control of a quadrotor aerial vehicle with input constraints and uncertain parameters. *Int J Control 2018; 91: 1140–1160*.
6. Mohd Basri MA, Husain AR and Danapalasingam KA. Intelligent adaptive backstepping control for MIMO uncertain non-linear quadrotor helicopter systems. *Trans Inst Meas Control 2015; 37: 345–361*.
7. Abci B, Zheng G, Efimov D, et al. Robust altitude and attitude sliding mode controllers for quadrotors. *IFAC Papersonline 2017; 50: 2720–2725*.
8. Boudjedir H, Bouhali O and Rizoug N. Adaptive neural network control based on neural observer for quadrotor unmanned aerial vehicle. *Adv Robot 2014; 28: 1151–1164*.
9. Chovancova A, Fico T, Hubinsky P, et al. Comparison of various quaternion-based control methods applied to quadrotor with disturbance observer and position estimator. *Robot Autonom Syst 2016; 79: 87–98*.
10. Dong W, Gu GY, Zhu XY, et al. High-performance trajectory tracking control of a quadrotor with disturbance observer. *Sensors Actuat A-Phys 2014; 211: 67–77*.
11. Chen FY, Lei W, Zhang KK, et al. A novel nonlinear resilient control for a quadrotor UAV via backstepping control and nonlinear disturbance observer. *Nonlinear Dyn 2016; 85: 1281–1295*.
12. Hongjun M, Liu Y, Li T, et al. Nonlinear high-gain observer-based diagnosis and compensation for actuators and sensors faults in a quadrotor unmanned aerial vehicle. *IEEE Trans Ind Inform 2018; 23: 11–21*.
13. Ding L, Ma R, Wu HT, et al. Yaw control of an unmanned aerial vehicle helicopter using linear active disturbance rejection control. *Proc Inst Mech Eng I 2017; 231: 427–435*.
14. Al-Wais S, Khoo S, Lee TH, et al. Robust Ho cost guaranteed integral sliding mode control for the synchronization problem of nonlinear tele-operation system with variable time-delay. *ISA Trans 2018; 72: 25–36*.
15. Zakeri E, Moezi SA and Eghtesad M. Tracking control of ball on sphere system using tuned fuzzy sliding mode controller based on artificial bee colony algorithm. *Int J Fuzzy Syst 2018; 20: 295–308*.
16. Jia Z, Yu J, Mei Y, et al. Integral backstepping sliding mode control for quadrotor helicopter under external uncertain disturbances. *Aerosp Sci Technol 2017; 68: 299–307*.
17. Song C, Wei C, Yang F, et al. High-order sliding mode-based fixed-time active disturbance rejection control for quadrotor attitude system. *Electronics 2018; 7: 357*.
18. Ríos H, Falcón R, González OA, et al. Continuous sliding-mode control strategies for quadrotor robust tracking: real-time application. *IEEE Trans Ind Electron 2019; 66: 1264–1272*.
19. Wang B, Yu X, Mu L, et al. Disturbance observer-based adaptive fault-tolerant control for a quadrotor helicopter subject to parametric uncertainties and external disturbances. *Mech Syst Signal Process 2019; 120: 727–743*.
20. Anwar J and Malik FM. Performance of non-linear observers for closed loop terminal sliding mode control of quadrotor UAV. In: *Proceeding of 14th international Bhurban conference on applied science &technology,* Islamabad, Pakistan, 10–14 January, 2017, pp.244–252. IEEE.
21. Hua C-C, Wang K, Chen J-N, et al. Tracking differentiator and extended state observer-based nonsingular fast terminal sliding mode attitude control for a quadrotor. *Nonlinear Dyn 2018; 94: 1–12*.
22. Ke J, Chen K, Wang J, et al. Quadrotors finite-time formation by nonsingular terminal sliding mode control with a high-gain observer. In: *The Euro-China conference on intelligent data analysis and application*, 12–14 October 2018, pp.53–64. Springer.
23. Aghababa MP and Akbari ME. A chattering-free robust adaptive sliding mode controller for synchronization of two different chaotic systems with unknown uncertainties and external disturbances. *Appl Math Comput 2012; 218: 5757–5768*.
24. Wang L, Zheng X-l and Wang S-Y. A novel binary fruit fly optimization algorithm for solving the multidimensional knapsack problem. *Knowledge-Based Syst 2013; 48: 17–23*.
25. Ding L, Shan W-T and Zhou J-Y. A hybrid high-performance trajectory tracking controller for unmanned hexrotor with disturbance rejection. *Trans Can Soc Mech Eng 2018; 42: 239–251*.
26. Dong W, Gu GY, Zhu X, et al. Development of a quadrotor test bed—modelling, parameter identification, controller design and trajectory generation. *Int J Adv Robot Syst 2015; 12: 7–21*.
27. Guo Y, Jiang B and Zhang Y. A novel robust attitude control for quadrotor aircraft subject to actuator faults and wind gusts. *IEEE/CAA J Automat Sin 2018; 5: 292–300*.
28. Yu S, Yu X, Shirinzadeh B, et al. Continuous finite-time control for robotic manipulators with terminal sliding mode. *Automatica 2005; 41: 1957–1964*.
29. Gao Z. Scaling and bandwidth-parameterization based controller tuning. In: *Proceeding of the 2003 American control conference*, Boston, MA, USA, 2003, pp.4989–4996.
30. Zheng ZW and Sun L. Adaptive sliding mode trajectory tracking control of robotic airships with parametric uncertainty and wind disturbance. *J Franklin Inst-Eng Appl Math 2018; 355: 106–122*.

31. Feng Y, Yu X and Man Z. Non-singular terminal sliding mode control of rigid manipulators. *Automatica 2002; 38: 2159–2167*.
32. Zheng EH and Xiong JJ. Quad-rotor unmanned helicopter control via novel robust terminal sliding mode controller and under-actuated system sliding mode controller. *Optik 2014; 125: 2817–2825*.
33. Nekoukar V and Erfanian A. Adaptive fuzzy terminal sliding mode control for a class of MIMO uncertain nonlinear systems. *Fuzzy Sets Syst 2011; 179: 34–49*.
34. Pan QK, Sang HY, Duan JH, et al. An improved fruit fly optimization algorithm for continuous function optimization problems. *Knowledge-Based Sys 2014; 62: 69–83*.
35. Li JQ, Pan QK and Mao K. A hybrid fruit fly optimization algorithm for the realistic hybrid flowshop rescheduling problem in steelmaking systems. *IEEE Trans Automat Sci Eng 2016; 13: 932–949*.
36. Rene B-C and Marta M. Optimal LQG controller for variable speed wind turbine based on genetic algorithms. *Energy Procedia 2012; 20: 207–216*.
37. Chen J. Four rotor aircraft the simulation research of automatic control. *Chin Comput Simul 2015; 32: 88–91*.
38. Li J, Qi X, Xia Y, et al. On linear/nonlinear active disturbance rejection switching control. *Acta Automatica Sinica 2016; 42: 202–212*.
39. APM2 Simulink Blockset [Online]. Available at: https://ww2.mathworks.cn/matlabcentral/fileexchange/39037-apm2-simulink-blockset?requestedDomain=zh (accessed 13 November 2012).

Appendix 1. The structure of ESO

The ESO is designed as

$$\begin{cases} e = z_1 - y \\ \dot{z}_1 = z_2 - \beta_1 e \\ \dot{z}_2 = z_3 - \beta_2 fal(e, \alpha_1, \delta) + b_0 u \\ \dot{z}_3 = -\beta_3 fal(e, \alpha_2, \delta) \end{cases} \tag{53}$$

where $z_i (i = 1, 2, 3)$ is the observed vectors of the state variable $x_i (i = 1, 2, 3)$. $\beta_i (i = 1, 2, 3)$ is gain and e is the variable error. *fal* is a saturation function that can eliminate the chattering. The mathematical description of *fal* is given by

$$fal(e, \alpha, \delta) = \begin{cases} \dfrac{e}{\delta^{1-\alpha}}, |e| \le \delta \\ |e|^{\alpha} \text{sign}(e), |e| > \delta \end{cases} \tag{54}$$

where δ is a positive parameter between 0 and 1.

Table 5. Optimal control parameters for SMC-LESO.

Parameter	Value	Parameter	Value
$\omega_{o-\phi}$	504.43	c_ϕ	1.5512
$\omega_{o-\theta}$	377.50	c_θ	5.9390
$\omega_{o-\psi}$	161.69	c_ψ	1.0448
k_ϕ	230.07	k_ψ	114.40
k_θ	320.47	/	/

Table 6. Optimal control parameters for LADRC.

Parameter	Value	Parameter	Value
$\omega_{o-\phi}$	809.173	$\omega_{c-\phi}$	269.21
$\omega_{o-\theta}$	673.475	$\omega_{c-\theta}$	204.92
$\omega_{o-\psi}$	630.92	$\omega_{c-\psi}$	338.05

Appendix 2. The parameters of SMC-LESO and LADRC

Both SMC-LESO and LADRC have the LESO defined in (12). Their control laws are given as follows

$$u_{\text{SMC–LESO}} = \frac{1}{b}(-kS - c\dot{e} + \ddot{x}_r - \hat{x}_3) \tag{55}$$

$$u_{\text{LADRC}} = \frac{\omega_c{}^2(x_r - \hat{x}_1) - 2\omega_c \hat{x}_2 - \hat{x}_3}{b} \tag{56}$$

The relevant control parameters are listed in Tables 5 and 6.